Construction of a lung adenocarcinoma prognostic model based on N6-methyl-adenosine-related long noncoding RNA and screening of potential drugs based on this model

Qinghua Hou[a], Yanfeng Zhong[b], Linzhuang Liu[c], Liusheng Wu[c] and Jixian Liu[c]

Lung adenocarcinoma (LUAD) has a high mortality rate. N6-methyl-adenosine (m6A)-related long noncoding RNA (lncRNA) is associated with tumor prognosis. Our objective was to construct an m6A-related lncRNA prognostic model and screen potential drugs for the treatment of LUAD. The LUAD sequencing data were randomly divided into Train and Test cohorts. In the Train group, the LASSO Cox regression was used to construct the m6A-related lncRNA prognostic model. The LUAD tumor immune dysfunction and exclusion model was used to evaluate immunotherapy efficacy in LUAD. The 'pRRophetic' package was utilized to screen potential drugs for the treatment of LUAD. Eleven m6A-related lncRNAs were identified by LASSO Cox regression and were used to construct the risk model to calculate sample risk scores. Patients were divided into high- and low-risk groups based on their median risk scores. The LUAD data of The Cancer Genome Atlas database showed that the overall survival (OS) of the high-risk group was significantly lower than that of the low-risk group in both cohorts. Multivariate Cox regression analysis showed that this risk model could serve as an independent prognostic factor of LUAD, and receiver operating characteristic curves suggested that m6A-related lncRNA prognostic signature has a good ability in predicting OS. Finally, nine potential drugs for LUAD treatment were screened based on this prognostic model. The prognostic model constructed based on the m6A-related lncRNAs facilitated prognosis prediction in LUAD patients. The screened therapeutic agents have potential application values and provide a reference for the clinical treatment of LUAD.
Anti-Cancer Drugs **33: 371–383**

Anti-Cancer Drugs 2022, **33**:371–383

Keywords: long noncoding RNA, lung adenocarcinoma, N6-methyl-adenosine, potential drugs, prognostic model

[a]Department of Clinical Medicine, Weifang Medical University, Weifang and Departments of [b]Central Laboratory and [c]Thoracic Surgery, Peking University Shenzhen Hospital, Shenzhen, China

Correspondence to Jixian Liu, PhD, Department of Thoracic Surgery, Peking University Shenzhen Hospital, Shenzhen, Guangdong 518036, China
Tel: +86 13923831537; e-mail: 252110465@qq.com

Received 2 February 2022 **Revised form accepted** 3 February 2022

Introduction

According to recent statistics published in 2020, lung cancer is the deadliest and second most common cancer worldwide, with a diagnosis rate of 11.4% [1]. Lung cancer is usually divided into small cell lung cancer and nonsmall cell lung cancer according to cytological type, and the most common subtype of nonsmall cell lung cancer is lung adenocarcinoma (LUAD) [2]. Owing to the lack of tumor-specific clinical symptoms experienced by LUAD patients in the early stage, they are often in the middle and late stages when diagnosed. By this time, local invasion or even distant metastasis has occurred in the tumor foci, the curative effect is poor, and the 5-year overall survival (OS) rate is less than 20% [3,4]. Targeted therapy and immunotherapy are two of the main methods of LUAD treatment. Although dozens of gene-targeted drugs such as EGFR, ALK, ROS1, BRAF, RET, etc., which are widely used, have achieved good clinical efficacy [5,6], the number of clinically available molecular targets is still limited, resulting in a limited number of beneficiaries [7,8]. In consideration of the limitations of LUAD treatment, new therapeutic targets are required to increase the clinical efficacy of LUAD treatment. Therefore, there is an urgent need for a reliable and new prognostic model, so as to provide reference for the clinical treatment of LUAD and improve the feasibility of targeted therapy.

N6-methyl-adenosine (m6A) is one of the most common mRNA modifications in eukaryotes and plays a key role in cancer pathogenesis [9]. It is mainly and dynamically regulated by methyltransferase (also referred to as 'writers'), demethylase (also referred to as 'erasers') and methylated binding protein (also referred to as 'readers') [10]. 'Writers' catalyze the transfer of methyl groups to adenosine bases, and 'erasers' refer to two demethylases, alpha-ketoglutarate-dependent dioxygenase (FTO) and

Supplemental Digital Content is available for this article. Direct URL citations appear in the printed text and are provided in the HTML and PDF versions of this article on the journal's website, www.anti-cancerdrugs.com.

 DOI: 10.1097/CAD.0000000000001277

alkane hydroxylase gene homolog 5 (ALKBH5), which remove m6A from RNA. 'Readers' recognize and bind to the m6A binding site, thereby generating the corresponding biological signal. Growing evidence suggests that m6A regulators are closely associated with malignancy [11,12]. For instance, in liver cancer, the downregulation of METTL14, which is one of the m6A 'writers', is significantly associated with tumor metastasis [13]. YTHDF, which is one of the 'readers', is associated with tumorigenicity and tumor stem cell-like activity in colorectal cancer [14]. FTO is one of the 'erasers', and it is carcinogenic in acute myeloid leukemia [15].

The coding of RNA is regulated by m6A, which also modifies long noncoding RNAs (lncRNAs). The latter, lncRNAs, is a class of noncoding RNAs with a length greater than 200 nucleotides and can control genetic expression, biological functions of cells, etc. [16]. Studies conducted in recent years showed that m6A influences lncRNAs mainly through two types of regulatory mechanisms. On one hand, m6A could induce the binding of RNA-binding protein, by providing binding sites for reader proteins or by regulating the structure of local RNAs. On the other hand, m6A might also regulate lncRNAs and specific DNA, by affecting the RNA-DNA triple helix structural relationship between sites [17]. Studies have shown that m6A affects the biological process (BP) of tumors by regulating related lncRNAs, such as lncRNA (LINC00958) as a competing endogenous RNA binds to miR-3619-5p to increase the expression of hepatocellular carcinoma-derived growth factors (HDGFs), whereas MET-TL3 can positively regulate the lncRNA LINC00958/miR-3619-5p/HDGF axis through m6A, thereby affecting the incidence and development of liver cancer [18]. However, m6A-related lncRNAs are less studied in LUAD, so we systematically analyzed m6A-related lncRNAs, constructed a prognostic model based on these lncRNAs, studied the correlation between lncRNAs and the tumor immune microenvironment, and screened for potential therapeutic agents for LUAD, based on this model.

Materials and methods

Data collection and screening of N6-methyl-adenosine-related lncRNAs

We downloaded LUAD transcriptome data and corresponding clinical data in FPKM format from The Cancer Genome Atlas (TCGA) database, as well as nucleotide variation (version calculated by 'varscan' software) data of LUAD samples, which included 535 cases of tumor samples and 59 cases of normal samples. In addition, we extracted 23 genes involved in m6A methylation from published literature [9,11,12,19–21]. The R software (version 4.1.3) was used to screen for lncRNAs from the TCGA transcriptome data, and the 'limma' package was used for m6A coexpression analysis to screen for lncRNAs related to m6A genes. The LUAD transcriptome data were merged with the corresponding clinical data. In the process of model construction, tumor samples with incomplete survival time or status information were removed, and in the correlation analysis of the clinicopathological characteristics of LUAD patients, 'unknown', 'TX', 'NX', and 'MX' were excluded samples.

Construction of prognostic model

The LUAD samples were randomly divided into Train and Test cohorts, each of which accounted for 50% of the data. The clinical characteristics of the two groups were statistically analyzed to determine whether there was any deviation between the two groups. Based on the LUAD samples in the Train cohort and their corresponding survival data, the genes associated with prognosis were screened from the m6A-related lncRNAs that were screened previously. Univariate Cox regression analysis was used for these lncRNAs, and the P threshold was set to 0.05 to prevent overfitting in the Cox regression model modeling process. The 'glmnet' software package was used to perform LASSO regression analysis on prognosis-related genes, and the cross-validation method was used to select the point with the smallest error as the penalty parameter 'λ' to determine the number of lncRNAs and the corresponding risk coefficients for building the model. The risk score formula is as follows: Risk Score = $\sum_i^n Xi \times Yi$ (n: number of lncRNAs, X: risk factor, and Y: level of gene expression).

Evaluation and testing of the prognostic model

We divided patients in the Train cohort into high- and low-risk subgroups based on the median risk score of the prognostic model. The 1-, 3-, and 5-year receiver operating characteristic (ROC) curve analyses and multi-index ROC curve analysis were then performed using the 'survival', 'survminer', and 'timeROC' packages in the R software to evaluate the predictive ability of this prognostic model for OS in patients with LUAD. The genes for which the model was constructed were subjected to principal component analysis (PCA) analysis by the 'prcomp' function in the 'Rtsne' package, and the OS of the two groups was compared by Kaplan–Meier analysis. In order to validate m6A-related lncRNA prognostic signature (m6A-LPS), we applied the Test cohort data to validate the constructed model. In addition, to verify whether the model was applicable to patients in different clinical groups, we also performed clinical group validation.

Functional enrichment and immune function analysis of differential genes

Differentially expressed genes (DEGs) between high- and low-risk groups of LUAD were screened according to the criteria of false discovery rate (FDR) < 0.05 and $|\log2FC| \geq 1$. Based on these DEGs, the 'clusterProfiler' package [22] and the 'GOplot' package [23] were used to perform gene ontology (GO) enrichment analysis and kyoto encyclopedia of genes and genomes (KEGG) analysis of DEGs from three aspects: BPs, cellular

components, and molecular functions. Pathway analysis and enrichment analysis were combined with logFC analysis. The single sample gene set enrichment analysis was then performed using the 'gsva' package to calculate immune cell infiltration scores and assess the immune-related pathway activity.

Mutation burden analysis

Based on the downloaded LUAD nucleotide variation data, we applied the Perl software (version 5.30.0) to calculate the genetic mutation burden of LUAD samples. Differences in tumor mutational burden of LUAD patients between high- and low-risk groups were analyzed using the 'limma' software package. Then, according to the patient's tumor mutation burden, all LUAD patients were divided into two groups with high and low mutation burdens, and combined with high- and low-risk groups, the 'survival' and 'survminer' packages were used to perform a combined survival analysis of the patient's tumor mutation burden and risk grouping.

Analysis of lung adenocarcinoma immunotherapy and screening of potential drugs

The tumor immune dysfunction and exclusion (TIDE) scoring file was obtained from the TIDE website (http://tide.dfci.harvard.edu). The TIDE score was used to evaluate the immune escape of the high- and low-risk groups, so as to determine the efficacy of immunotherapy in the high- and low-risk groups. The 'pRRophetic' package [24] was subsequently applied to screen potential therapeutic drugs for LUAD.

Results

N6-methyl-adenosine-related lncRNAs

Among the m6A genes extracted from the published literature, there were eight 'writers' genes (METTL3, METTL14, METTL16, WTAP, VIRMA, ZC3H13, RBM15, and RBM15B), 13 'readers' genes (YTHDC1, YTHDC2, YTHDF1, YTHDF2, YTHDF3, HNRNPC, FMR1, LRPPRC, HNRNPA2B1, IGFBP1, IGFBP2, IGFBP3, and RBMX), and two 'erasers' genes (FTO and ALKBH5). A total of 1126 m6A-related lncRNAs were screened by coexpression analysis (Supplementary Table 1, supplemental digital content 1, http://links.lww.com/ACD/A424), and the correlation filtering criteria were: correlation > 0.6; $P < 0.001$ (Fig. 1).

Construction of N6-methyl-adenosine-related lncRNA prognostic model

After performing Chi-square test, it was found that there was no deviation in the clinical characteristics of the patients in the Train cohort and the Test cohort ($P > 0.05$; Table 1). We used univariate Cox regression analysis to obtain 35 lncRNAs related to prognosis in the Train group (Fig. 2a) and obtained 20 lncRNAs related to prognosis through LASSO regression analysis. Then, we used multivariate Cox regression analysis to analyze the lncRNAs obtained by LASSO regression after optimization, and 11 lncRNAs (AP001178.1, AL121772.2, AL360270.2, AL358115.1, AF131215.5, AC010999.2, TRAF3IP2-AS1, AC026355.2, ADPGK-AS1, LINC02656, and AC012409.4) were used to construct the prognostic model (Fig. 2b and c). According to the constructed risk score formula, the risk scores of the samples in the Train cohort and the Test cohort were calculated, respectively. The calculation method of the risk score was as follows: Risk Score = 1.828*EXP(AP001178.1) + 0.871*EXP(AL121772.2) + 1.365*EXP(AL360270.2) + 1.458*EXP(AL358115.1) + (−0.499)*EXP(AF131215.5) + (−2.683)*EXP(AC010999.2) + (−1.849)*EXP(TRAF3IP2-AS1) + (−0.3383914)*EXP(AC026355.2) + (−4.597)*EXP(ADPGK-AS1) + (−1.131)*EXP(LINC02656) + 1.762*EXP(AC012409.4). In addition, we also performed m6A correlation analysis on these lncRNAs (red represents positive correlation and blue represents negative correlation; see Fig. 2d).

Prognostic ability of the N6-methyl-adenosine-related lncRNA prognostic model

In the Train cohort, we divided the samples into high- and low-expression groups based on the median risk score and then performed PCA based on model m6A-related lncRNAs, m6A all-related lncRNAs, m6A genes, and all genes, and the results showed that in the m6A-related lncRNAs, the high-risk group and the low-risk group had the most obvious differentiation (Fig. 3). This showed that the model we had constructed could differentiate between high- and low-risk groups very well. We also explored the difference in OS between the high- and low-risk groups in the Train and Test cohorts by Kaplan–Meier analysis, and the OS time in the high-risk group was significantly shorter than that in the low-risk group ($P < 0.001$; Fig. 4). We also plotted risk curves based on the risk scores, in both the Train and Test cohorts, patients in the high-risk group had more deaths and shorter survival times compared with the low-risk group (Fig. 5a–f, on the right side of the dotted line), and the expression of lncRNAs involved in the model construction in high- and low-risk groups was also displayed in the form of a heat map, among which the expression levels of AP001178.1, AL121772.2, AL360270.2, AL358115.1, and AC012409.4 increased, as the risk scores increased. The expression levels of AF131215.5, AC010999.2, TRAF3IP2-AS1, AC026355.2, ADPGK-AS1, and LINC02656 were significantly higher in the low-risk group and were the low-risk genes in this model (Fig. 5g–i). In addition, we also conducted a validation analysis in each clinical subgroup of all patients, with different ages (age ≤ 65 and age > 65), sex (female and male), and pathological stage (stages I–II and stages III–IV). The OS of the low-risk group was significantly better than that of the high-risk group ($P < 0.05$; Fig. 6a–f), indicating that the model is suitable for patients with different clinical subgroups. Subsequently, applying ROC analysis to evaluate the sensitivity and specificity of the prognostic model, we found that the ROC area under the curve (AUC) was 0.729

Fig. 1.

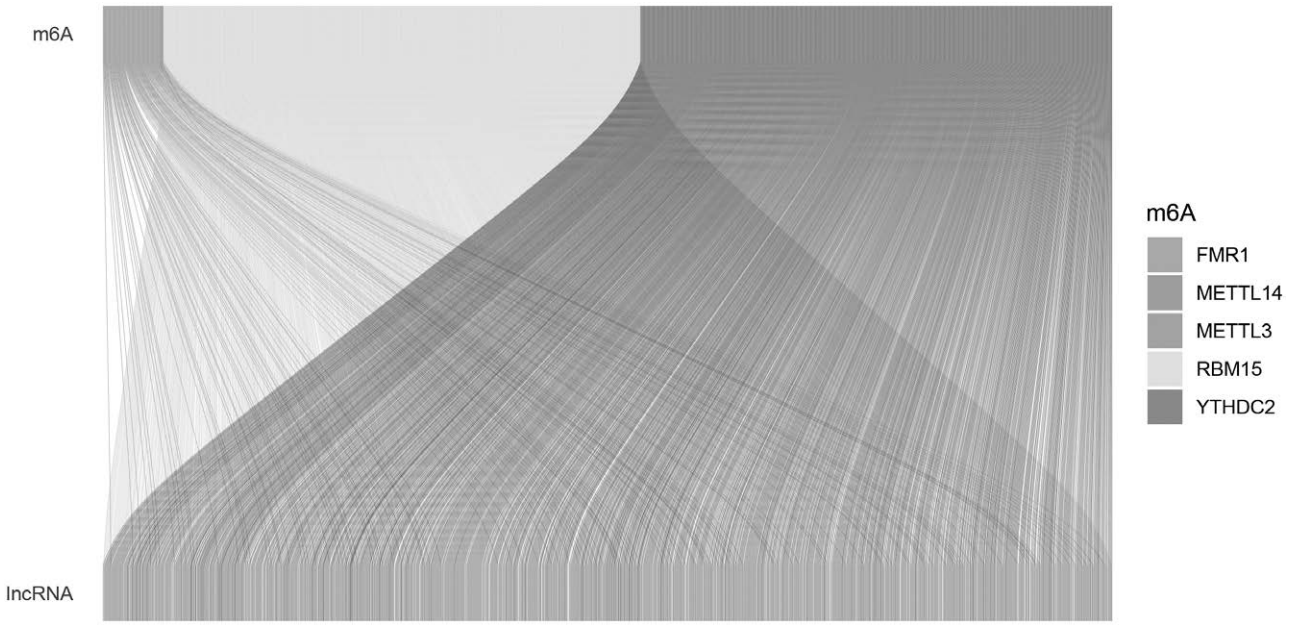

N6-methyl-adenosine-related lncRNA, correlation coefficient > 0.6, $P < 0.001$.

Table 1. Clinical and statistical analysis of lung adenocarcinoma lung adenocarcinoma patients in the train and test cohorts

Covariates	Type	Total	Test	Train	*P* value
Age	<=65	224(47.86%)	106(45.69%)	118(50%)	0.3979
	>65	234(50%)	121(52.16%)	113(47.88%)	
	Unknow	10(2.14%)	5(2.16%)	5(2.12%)	
Sex	Female	254(54.27%)	135(58.19%)	119(50.42%)	0.1111
	Male	214(45.73%)	97(41.81%)	117(49.58%)	
Stage	Stage I	253(54.06%)	127(54.74%)	126(53.39%)	0.8899
	Stage II	107(22.86%)	53(22.84%)	54(22.88%)	
	Stage III	75(16.03%)	34(14.66%)	41(17.37%)	
	Stage IV	25(5.34%)	13(5.6%)	12(5.08%)	
	Unknow	8(1.71%)	5(2.16%)	3(1.27%)	
T	T1	159(33.97%)	82(35.34%)	77(32.63%)	0.6988
	T2	248(52.99%)	123(53.02%)	125(52.97%)	
	T3	39(8.33%)	16(6.9%)	23(9.75%)	
	T4	19(4.06%)	9(3.88%)	10(4.24%)	
	Unknow	3(0.64%)	2(0.86%)	1(0.42%)	
M	M0	315(67.31%)	161(69.4%)	154(65.25%)	1
	M1	24(5.13%)	12(5.17%)	12(5.08%)	
	Unknow	129(27.56%)	59(25.43%)	70(29.66%)	
N	N0	302(64.53%)	145(62.5%)	157(66.53%)	0.3275
	N1	86(18.38%)	49(21.12%)	37(15.68%)	
	N2	66(14.1%)	28(12.07%)	38(16.1%)	
	N3	2(0.43%)	1(0.43%)	1(0.42%)	
	Unknow	12(2.56%)	9(3.88%)	3(1.27%)	

at 1 year, 0.689 at 2 years, and 0.725 at 3 years (Fig. 6g), indicating that the model has a certain predictive capability.

Analysis of risk score and independent prognostic factors

Next, we performed a univariate analysis in all LUAD patients based on the model-based risk score and clinical characteristics such as age, sex, and stage, and the results showed that stage and risk score had a significant effect on prognosis (Fig. 7a). The results of multivariate analysis showed that risk score and stage still had significant prognostic significance (Fig. 7b), indicating that risk score could be used as an independent prognostic factor for patients with LUAD. In addition, we also conducted a multi-index ROC curve analysis. The multiple curves in the figure represent the risk scores and clinical characteristics of LUAD patients. The AUC of each clinical characteristic was 0.537 for age, 0.596 for sex, and 0.711 for stage, whereas the AUC of the model-based risk value was 0.729, which indicated that our constructed LUAD

Fig. 2.

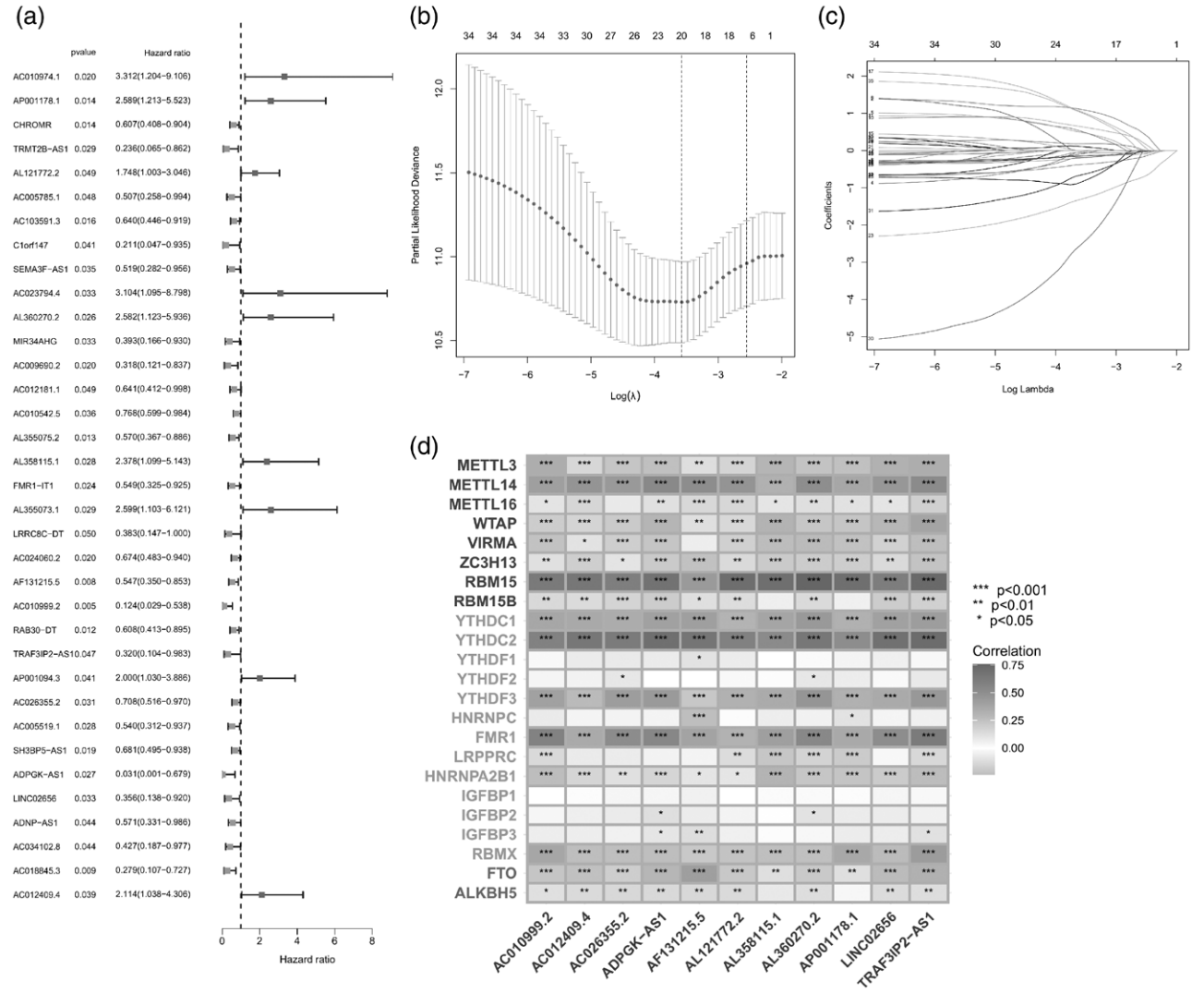

Construction of risk signature. (a) 33 lncRNAs associated with lung adenocarcinoma (LUAD) prognosis, $P < 0.05$. (b) LASSO Cox regression analysis of prognostic m6A-related lncRNAs. (c) Correlation between m6A genes and lncRNAs involved in model construction.

prognostic model was superior to other clinical features in predicting patient survival (Fig. 7c). Moreover, we drew the c-index curve to the same conclusion (Fig. 7d). The above evaluation indicated that our model based on m6A-related lncRNAs could serve as an independent prognostic factor for LUAD.

Analysis of gene ontology/kyoto encyclopedia of genes and genomes enrichment and immune function

To further explore the functions and pathways of differential genes between the high- and low-risk groups in all TCGA-LUAD samples, we used the 'limma' R package to extract DEGs with filtering conditions of FDR < 0.05 and |log2FC| ≥ 1. A total of 223 DEGs were identified between the high- and low-risk groups, of which 82 genes were upregulated and 141 genes were downregulated in the high-risk group (Supplementary Table 2, supplemental digital content 2, http://links.lww.com/ACD/A425). GO-enrichment analysis and KEGG pathway analysis were then performed based on these DEGs. GO-enrichment analysis showed that DEGs were mainly associated with spliceosomal tri-snRNP complex assembly, formation of quadruple SL/U4/U5/U6 snRNP, mRNA trans splicing via spliceosome, Golgi lumen, endopeptidase inhibitor activity, peptidase inhibitor activity, etc. KEGG-enrichment analysis showed that DEGs were mainly involved in the nitrogen metabolism pathway (Table 2, Fig. 8a). A subsequent analysis of differences in immune function showed that there were significant differences in type II IFN response, type I IFN response, HLA, antigenpresenting cells (APC) co-stimulation, APC coinhibition, chemokine receptor, parainflammation, cytolytic activity, inflammation-promoting, T

Fig. 3.

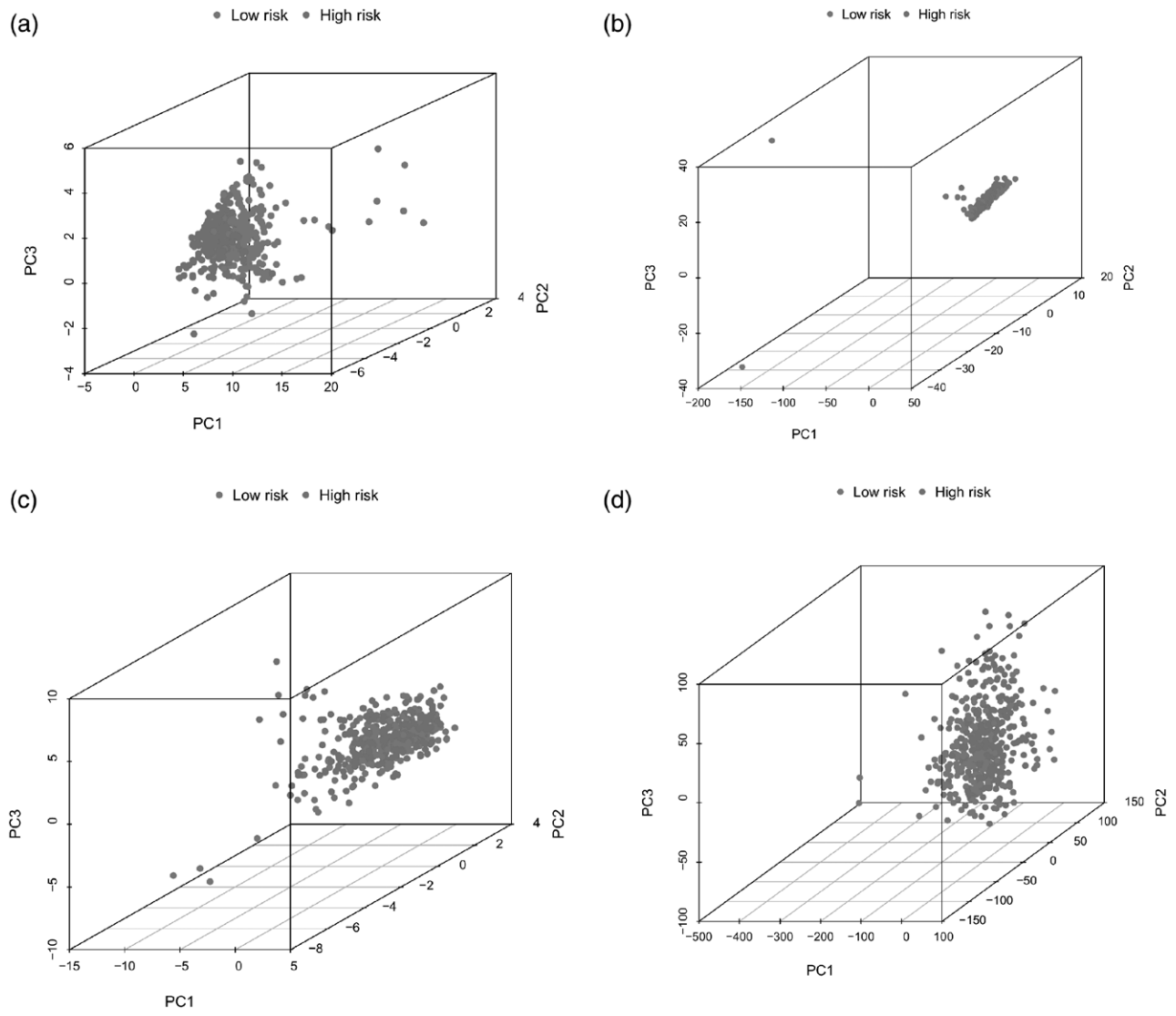

Principal component analysis (PCA). (a) PCA analysis of m6A-related lncRNAs used in constructing the prognostic model. (b) PCA analysis of all m6A-related lncRNAs. (c) PCA analysis of 23 m6A-related lncRNAs. (d) PCA analysis of all genes based on TCGA-LUAD data.

cell coinhibition, check-point, T cell costimulation, etc. (Fig. 8b, low expression in blue and high expression in red). It was found that these immune functions declined in the high-risk group.

Analysis of lung adenocarcinoma tumor mutation

In order to explore the mutation differences between samples in the high- and low-risk groups, we first analyzed the mutation frequency of the different groups. The results showed that the overall mutation frequency of samples in the high-risk group (93.44%) was higher than that in the low-risk group (83.33%). Hence, this showed that the high-risk group based on the prognostic model was accompanied by a higher mutation frequency, of which TP53 had the highest mutation frequency in the low-risk group, whereas titin (TTN) had the highest mutation frequency (50%) in the high-risk group. We also found that the frequency of TP53 mutation was not different between the high- and low-risk groups and was dominated by Missense Mutation, and the mutation information was displayed in the form of waterfall plots (Fig. 9a and b). We then performed a mutational load differential analysis, again with significant differences between the high- and low-risk groups, with a significantly higher mutational load in the high-risk group than that in the low-risk group (Fig. 9c). Then, we carried out a survival analysis of tumor mutation burden in combination with high- and low-risk

Fig. 4.

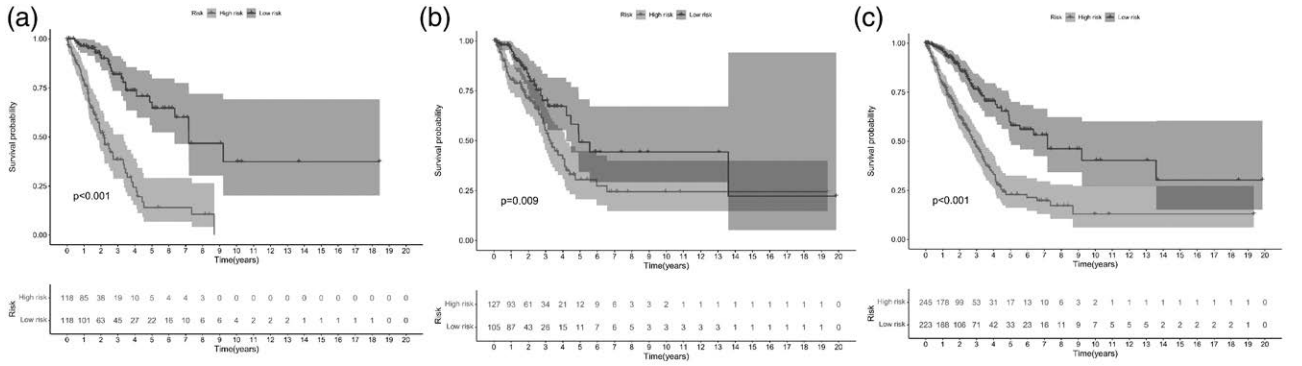

Evaluation of model-based survival time. (a) Kaplan–Meier curves of the overall survival of high- and low-risk patients in the Train cohort. (b) Kaplan–Meier curves of the overall survival of high- and low-risk patients in the Test cohort. (c) Kaplan–Meier curves of the overall survival of all high- and low-risk lung adenocarcinoma (LUAD) patients.

Fig. 5.

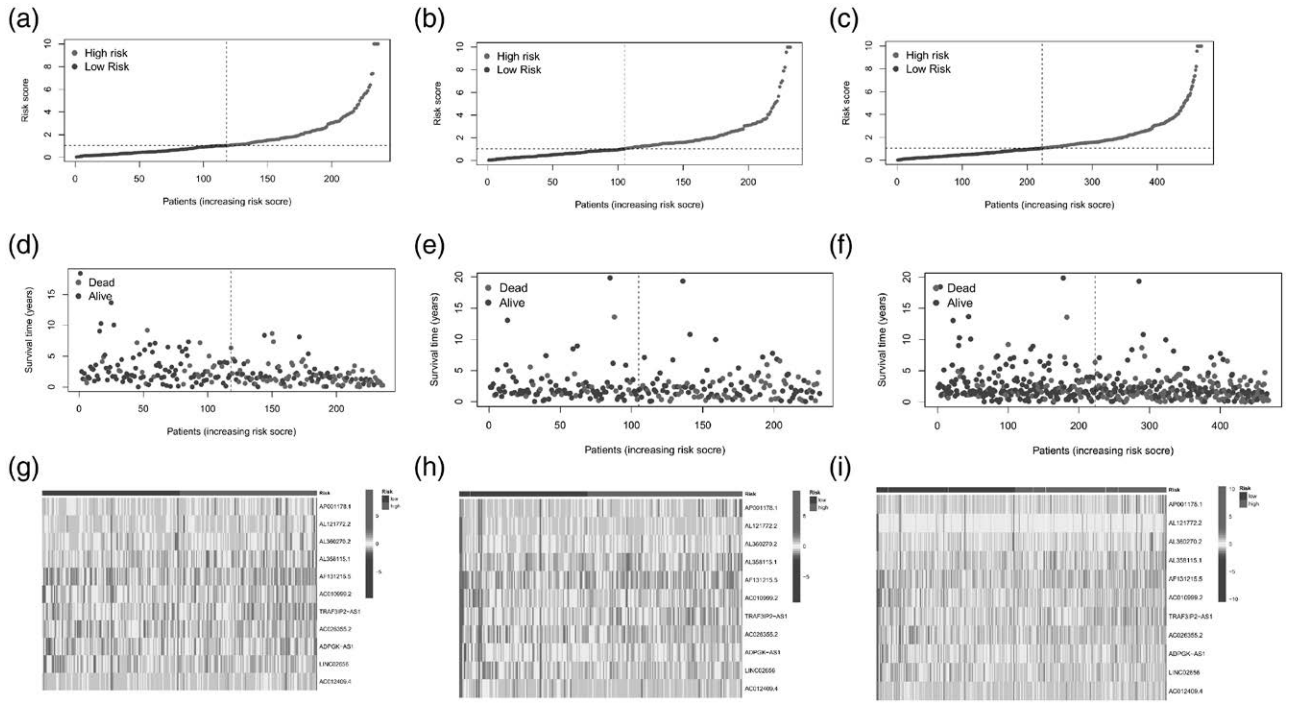

Evaluation of the risk curves of the model. (a) Distribution of patients based on the risk score in the Train cohort. (b) Distribution of patients based on the risk score in the Test cohort. (c) Distribution of patients based on the risk scores of all lung adenocarcinoma (LUAD) patients. (d) The survival status for each patient in the Train cohort (low-risk population: on the left side of the dotted line; high-risk population: on the right side of the dotted line). (e) The survival status for each patient in the Test cohort. (f) The survival status of all LUAD patients. (g) The heatmap of 11 m6A-related lncRNAs in the Train cohort. (h) The heatmap of 11 m6A-related lncRNAs in the Test cohort. (i) The heatmap of 11 m6A-related lncRNAs of all LUAD patients.

levels, determined the optimal cutoff value through the 'surv_cutpoint' function, and then divided the mutation data into two groups of high- and low-mutation 'high-tumor mutation burden' 'L'. Combined with the high- and low-risk groups, they were divided into four groups for survival analysis. The results showed that there was no significant difference in the OS of patients between the high- and low-burden mutation groups (Fig. 9d), whereas after combining the high- and low-risk groups, there was a significant difference in survival time of the patients between the four groups (Fig. 9e).

Fig. 6.

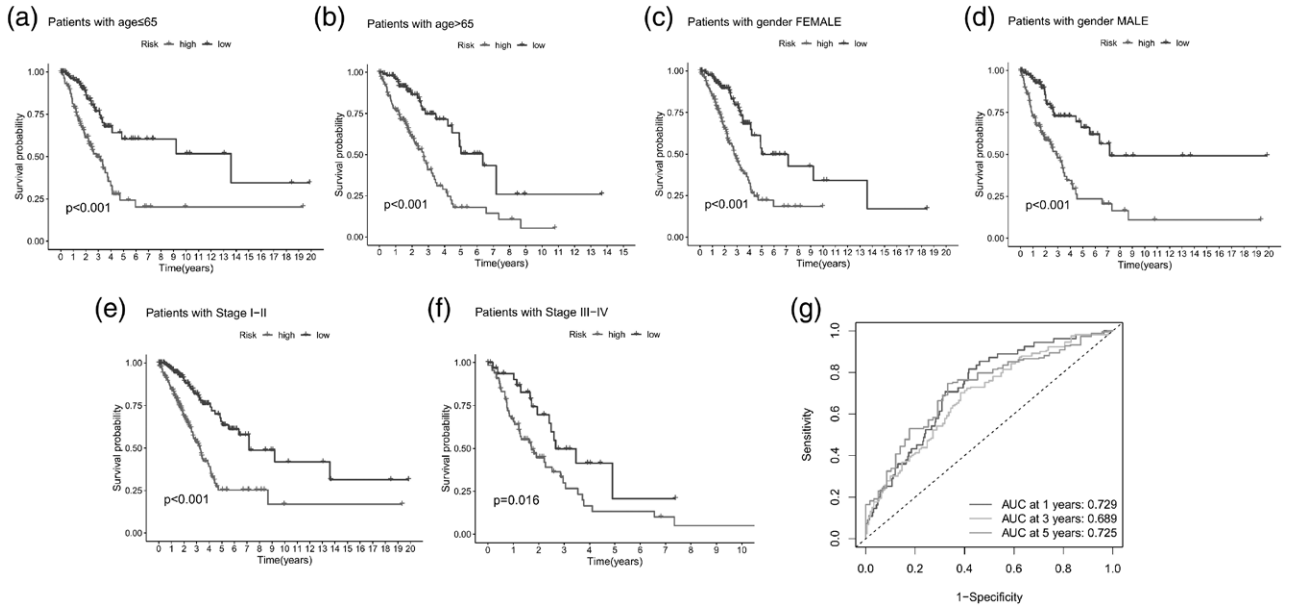

Stratification analysis of survival according to the clinicopathological characteristics and receiver operating characteristics (ROC) curve analysis of prognostic model. (a and b) Survival analysis of all patients adjusted to age, (c and d) sex, (e and f) pathological stage between high- and low-risk groups. (g) ROC curves of prognostic models.

Analysis of immunotherapy and screening of potential drugs for lung adenocarcinoma treatment

We analyzed the immune evasion and immunotherapy of LUAD samples by TIDE score, and the high-risk group had lesser potential for immune evasion and better effect of receiving immunotherapy (Fig. 10a). Using the pRRophetic package for predicting drug sensitivity, for those with different sensitivities between high- and low-risk groups, the lower the IC50 value, the more sensitive the drug. The results showed that ABT.263, ABT.888, AG.014699, AICAR, AP. 24534, AS601245, ATRA, AUY922, and AZD.0530 had significant differences in sensitivity between high- and low-risk groups, with the high-risk group being paired (Fig. 10b–j).

Discussion

LUAD has a high incidence and poor prognosis worldwide, and faces major challenges in early tumor screening, diagnosis, and treatment [25]. The abnormal regulation of lncRNAs is an important factor in tumorigenesis and development, and these lncRNAs were also potential diagnostic and therapeutic targets for LUAD. A growing number of studies have demonstrated that m6A modifications and lncRNAs are involved in regulating tumor initiation, progression, and prognosis through endogenous lncRNAs targeting m6A regulators [26]. Therefore, we established an m6A-related lncRNA signature to explore the potential prognostic markers and therapeutic targets in LUAD patients and predicted potential therapeutic drugs for LUAD based on these lncRNA signatures.

We collected the data of 535 LUAD patients from the TCGA dataset and identified 35 m6A-related lncRNAs associated with LUAD prognosis. Furthermore, we improved the prediction of OS in LUAD patients by incorporating 11 of the 35 m6A-related prognostic lncRNAs into m6A-LPS by LASSO Cox regression. Based on this model, the risk scores of LUAD patients were calculated, and these patients were divided into high- and low-risk groups according to the median risk score. We found that high risk was accompanied by poor OS, and the m6A-LPS risk score was determined by multivariate Cox regression analysis as an independent risk factor for OS. Then, we used time-dependent ROC curve, multi-index ROC curve, and C-index curve analyses to show that m6A-LPS has a certain predictive ability for the prognosis of LUAD and has higher accuracy than other clinical features. In order to validate whether the constructed model was suitable for patients in different clinical groups, we analyzed the patients in each clinical group based on the risk model. The results showed that the model was suitable for both male and female patients, patients aged ≤65 and >65 years old, and early- and late-stage patients, further demonstrating the predictive potential of the risk assessment model.

In subsequent mutational analysis, we found that patients in the high-risk group were accompanied by a higher mutation rate, with the highest frequency of TTN mutations in the high-risk group, TTN encodes a large

Fig. 7.

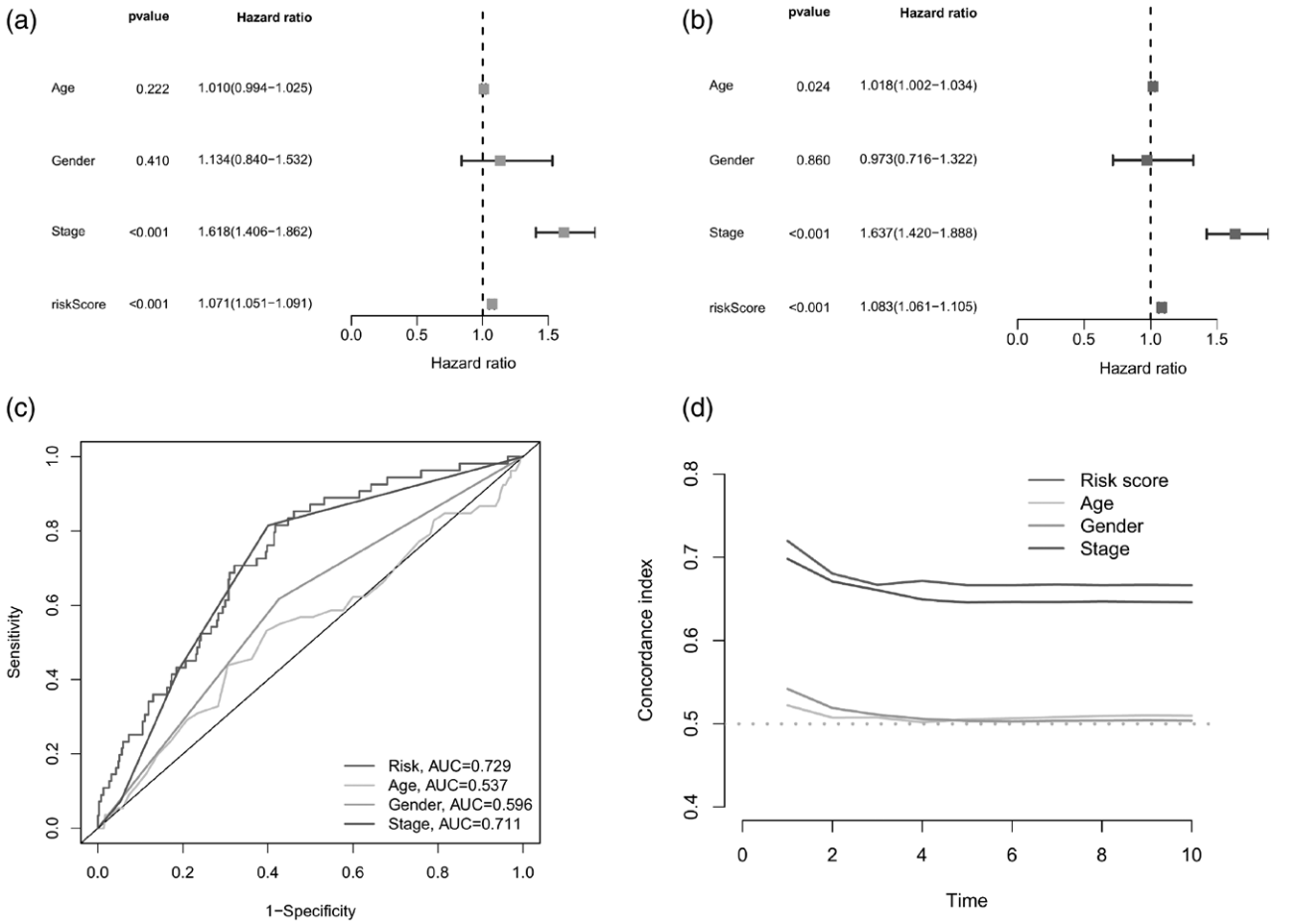

Analysis of prognostic factors. (a) Univariate prognostic factors analysis forest plot of the model for all lung adenocarcinoma (LUAD) patients. (b) Multivariate prognostic factors analysis forest plot of the model for all LUAD patients.

Table 2. Gene ontology/kyoto encyclopedia of genes and genomes enrichment analysis

Ontology	ID	Description	Gene ratio	Bg ratio	*P*.adjust	q value
BP	GO:0000244	Spliceosomal tri-snRNP complex assembly	5/154	26/18670	0.001	0.001
BP	GO:0000353	Formation of quadruple SL/U4/U5/U6 snRNP	4/154	12/18670	0.001	0.001
BP	GO:0000365	mRNA trans splicing, via spliceosome	4/154	12/18670	0.001	0.001
CC	GO:0005796	Golgi lumen	6/161	102/19717	0.028	0.026
CC	GO:0046540	U4/U6 x U5 tri-snRNP complex	4/161	42/19717	0.028	0.026
CC	GO:0097526	Spliceosomal tri-snRNP complex	4/161	42/19717	0.028	0.026
MF	GO:0004867	Serine-type endopeptidase inhibitor activity	7/130	94/17697	0.002	0.002
MF	GO:0004866	Endopeptidase inhibitor activity	8/130	175/17697	0.005	0.004
MF	GO:0030414	Peptidase inhibitor activity	8/130	182/17697	0.005	0.004
KEGG	hsa00910	Nitrogen metabolism	3/63	17/8076	0.035	0.034

BP, biological processes; CC, cellular components; GO, gene ontology; KEGG, kyoto encyclopedia of genes and genomes; MF, molecular functions.

abundant protein of striated muscle, which is closely related to actin and myosin and constitutes the third most abundant type of fiber in human heart and skeletal muscle [27]. Studies have shown that TTN is mutated in many types of tumors, including lung squamous cell carcinoma, LUAD, and colon adenocarcinoma [28], which is consistent with our findings.

In order to better guide the clinical treatment of LUAD, we screened nine potential drugs based on the constructed model, including ABT.263, ABT.888, AG.014699, AICAR, AP.24534, AS601245, ATRA, AUY922, and AZD.0530. ABT.263 is a Bcl-2 inhibitor, and oral administration of ABT.263 induces complete tumor regression in xenograft models of small cell lung cancer

Fig. 8.

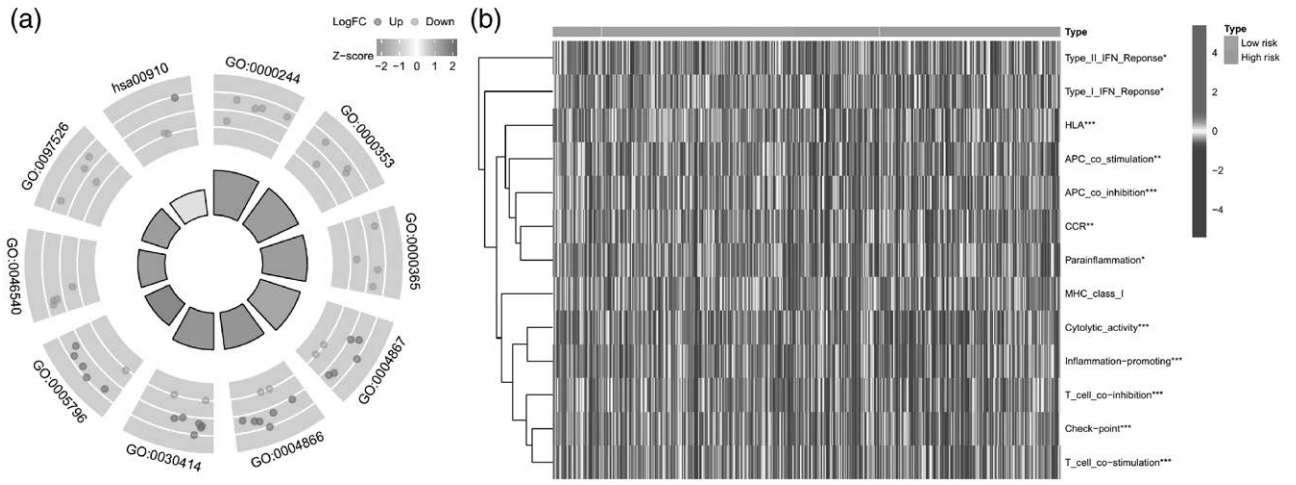

Analysis of GO/KEGG enrichment and immune functions. (a) Differentially expressed genes (DEGs) combined with logFC GO enrichment analysis and KEGG pathway, where the inner circle height is the relative size of p.adj, and the corresponding filled color represents the zscore value corresponding to the entry. The outer circle is the molecule contained in the entry, the height represents the corresponding logFC value, the molecule with positive logFC is marked as Up, and the molecule with negative logFC is marked as Down (see Table 2 for details). (b) Heatmap of immune functions.

Fig. 9.

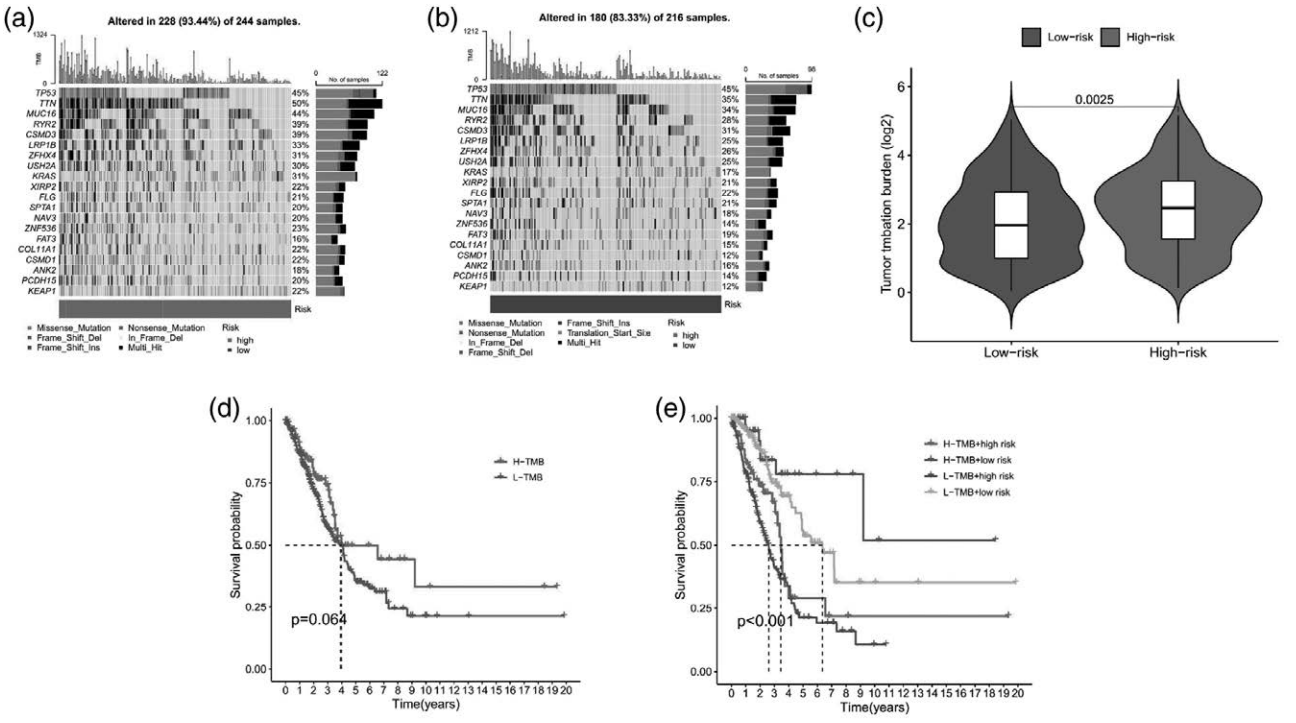

Model-based lung adenocarcinoma (LUAD) mutational burden and survival analysis. (a and b) Mutational signals of the high- and low-risk groups. (c) Grouped burden differences between high- and low-risk groups. (d and e) Combined survival analysis of high- and low-mutation groups and high- and low-risk groups.

Fig. 10.

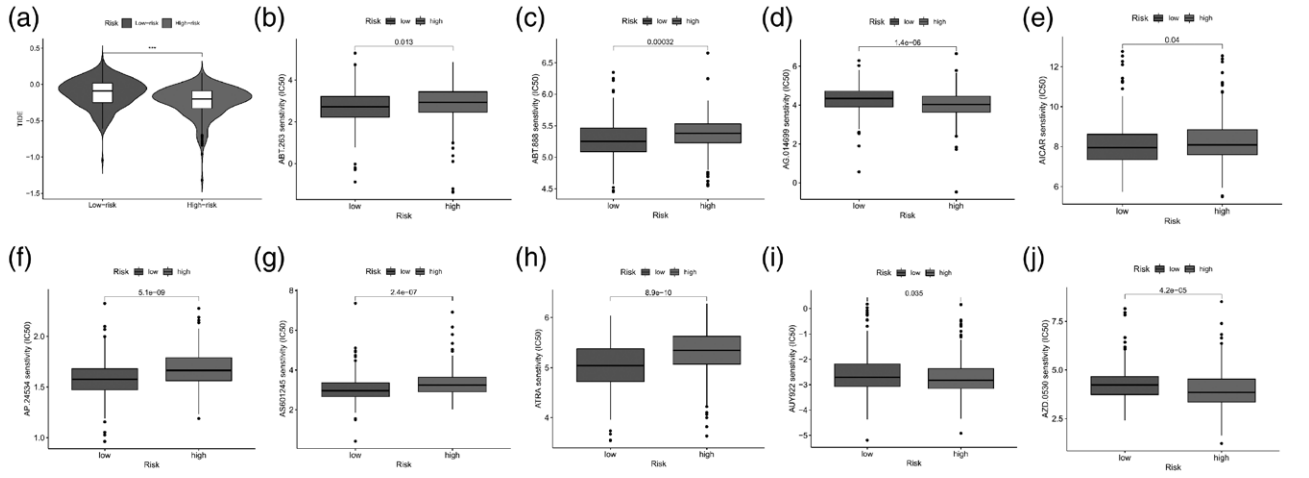

Immune evasion analysis and drug screening. (a) Immune evasion analysis. (b–j) Model-based screening of potential drugs.

and acute lymphoblastic leukemia [29]. The tumor suppressor genes BRCA1 and BRCA2 can repair DNA double-strand breaks through homologous recombination deficiency (HRD), and the loss of their functions could easily lead to gene instability, which in turn led to the generation of tumor cells [30]. Studies have shown that poly ADP-ribosylation polymerase (PARP) inhibitors are abnormally sensitive to BRCA1- and BRCA2-mutated tumor cells, so PARP inhibitors are used to treat HRD-deficient malignancies [31]. ABT.888 is an oral PARP inhibitor with the ability to inhibit poly ADP-ribose polymerase-1/2 (PARP-1/2) [32], whereas PARP-1/2 are involved in DNA breakage and PAR polymerization and play a key role in the base excision repair pathway [33]. AG.014699 is a potent PARP inhibitor codeveloped by Newcastle University and Agouron Pharmaceuticals (part of Pfizer GRD) [34]. AICAR (5-aminoimidazole-4-carboxamide riboside) is an AMP-activated protein kinase (AMPK) agonist [35,36]. There is growing evidence that this compound is cytotoxic to a variety of cancer cells, including colon and prostate cancer. Therefore, AICAR might be a promising anticancer drug [37–40], with potential value for the drug therapy of LUAD. AP.24534, also known as ponatinib, is a potent oral tyrosine kinase inhibitor with activity against unmutated and mutated BCR-ABL, including threonine at position 315 (T315I) Isoleucine mutation [41]. Ponatinib showed significant antileukemia activity in patients with Philadelphia chromosome (Ph)-positive disease [42]. c-Jun N-terminal kinase (JNK) is a subfamily of mitogen-activated protein kinases that regulate important cellular activities including cell proliferation, differentiation, and apoptosis [43]. JNK promotes the development of many cancers including lung cancer [44]. AS601245, a cell-permeable JNK inhibitor, showed promising anticancer effects in colon cancer and T-cell acute lymphoblastic leukemia [45]. Since ATRA was first used in the clinical treatment of acute promyelocytic leukemia, it has provided a successful example for ATRA in the treatment of malignant tumors. The research on the relationship between ATRA and tumor cells has increased yearly [46]. Studies have shown that ATRA has an inhibitory effect on the proliferation of lung cancer cells and solid tumor cells [47]. AUY922 is a newly developed nongeldanamycin HSP90 inhibitor. By inhibiting HSP90, AUY922 can overcome ALX-mediated lung cancer cell lines and lung cancer cells and drug resistance in animal models [48]. AZD0530 is an oral inhibitor of Src signaling pathway (Src is involved in tumor progression and metastasis). AZD0530 can significantly inhibit the motility and invasiveness of endocrine-resistant breast cancer cells *in vitro* [49]. In addition, the study by Zhao *et al.* [50] showed that AZD0530 could reduce the drug resistance of ALK-positive lung cancer cells by inhibiting the Src signaling pathway. The above nine drugs were all potential drugs for the clinical treatment of LUAD.

However, our study had some limitations. First, the model was only validated with TCGA's own data, and more external data validation based on RNA-seq cohorts is needed in the future. In addition, we only preliminarily explored the signaling pathways involved in the 11 m6A-related prognostic lncRNA targets and the correlation of m6A-related lncRNAs with immunity. However, the specific mechanisms of m6A-related lncRNAs in LUAD and their interconnections with immunity and m6A regulators remain to be not entirely clear, and more experiments are needed to validate our findings.

In summary, we constructed a prognostic model with 11 m6A-related lncRNAs, which was able to predict

the clinical progression and prognostic risks of LUAD. We screened for potential drugs and provided clinical reference for the treatment of LUAD using this model. Moreover, these lncRNAs might be valuable diagnostic candidates and prognostic biomarkers, as well as potential therapeutic targets for LUAD.

Acknowledgements

The authors would like to thank Editage for English language editing.

This work was supported by grants from the Science and Technology Innovation Committee of Shenzhen Municipality (Grant No. JCYJ20180228175531145) and the Open Foundation of Shenzhen Huada Institute of Life Sciences (Grant No. BGIRSZ20200003).

J.L. designed the research; Y.Z. guided the research; L.L. and L.W. collected and downloaded the data for our research; and Q.H. analyzed the data and wrote the paper. Patient data statement: our study does not contain data from any individual person or any animals.

Conflicts of interest

There are no conflicts of interest.

References

1 Sung H, Ferlay J, Siegel RL, Laversanne M, Soerjomataram I, Jemal A, *et al*. Global Cancer Statistics 2020: GLOBOCAN estimates of incidence and mortality worldwide for 36 cancers in 185 countries. *CA Cancer J Clin* 2021; **71**:209–249.
2 Hutchinson BD, Shroff GS, Truong MT, Ko JP. Spectrum of lung adenocarcinoma. *Semin Ultrasound CT MR* 2019; **40**:255–264.
3 Ettinger DS, Wood DE, Aisner DL, Akerley W, Bauman J, Chirieac LR, *et al*. Non-small cell lung cancer, Version 5.2017, NCCN clinical practice guidelines in oncology. *J Natl Compr Canc Netw* 2017; **15**:504–535.
4 Lu M, Tian Y, Yue WM, Li L, Li SH, Qi L, *et al*. GOLPH3, a good prognostic indicator in early-stage NSCLC related to tumor angiogenesis. *Asian Pac J Cancer Prev* 2014; **15**:5793–5798.
5 Osmani L, Askin F, Gabrielson E, Li QK. Current WHO guidelines and the critical role of immunohistochemical markers in the subclassification of non-small cell lung carcinoma (NSCLC): moving from targeted therapy to immunotherapy. *Semin Cancer Biol* 2018; **52**:103–109.
6 Xing P, Wang S, Wang Q, Ma D, Hao X, Wang M, *et al*. Efficacy of crizotinib for advanced ALK-rearranged non-small-cell lung cancer patients with brain metastasis: a multicenter, retrospective study in China. *Target Oncol* 2019; **14**:325–333.
7 Park JY, Jang SH. Epidemiology of lung cancer in Korea: recent trends. *Tuberc Respir Dis (Seoul)* 2016; **79**:58–69.
8 Testa U, Castelli G, Pelosi E. Lung cancers: molecular characterization, clonal heterogeneity and evolution, and cancer stem cells. *Cancers (Basel)* 2018; **10**:E248.
9 Niu Y, Zhao X, Wu YS, Li MM, Wang XJ, Yang YG. N6-methyl-adenosine (m6A) in RNA: an old modification with a novel epigenetic function. *Genomics Proteomics Bioinformatics* 2013; **11**:8–17.
10 Fang Q, Chen H. The significance of m6A RNA methylation regulators in predicting the prognosis and clinical course of HBV-related hepatocellular carcinoma. *Mol Med* 2020; **26**:60.
11 Chen XY, Zhang J, Zhu JS. The role of m6A RNA methylation in human cancer. *Mol Cancer* 2019; **18**:103.
12 Liu S, Li Q, Chen K, Zhang Q, Li G, Zhuo L, *et al*. The emerging molecular mechanism of m6A modulators in tumorigenesis and cancer progression. *Biomed Pharmacother* 2020; **127**:110098.
13 Ma JZ, Yang F, Zhou CC, Liu F, Yuan JH, Wang F, *et al*. METTL14 suppresses the metastatic potential of hepatocellular carcinoma by modulating N6 -methyladenosine-dependent primary MicroRNA processing. *Hepatology* 2017; **65**:529–543.
14 Bai Y, Yang C, Wu R, Huang L, Song S, Li W, *et al*. YTHDF1 regulates tumorigenicity and cancer stem cell-like activity in human colorectal carcinoma. *Front Oncol* 2019; **9**:332.
15 Li Z, Weng H, Su R, Weng X, Zuo Z, Li C, *et al*. FTO plays an oncogenic role in acute myeloid leukemia as a N6-methyladenosine RNA demethylase. *Cancer Cell* 2017; **31**:127–141.
16 Kopp F, Mendell JT. Functional classification and experimental dissection of long noncoding RNAs. *Cell* 2018; **172**:393–407.
17 Ma S, Chen C, Ji X, Liu J, Zhou Q, Wang G, *et al*. The interplay between m6A RNA methylation and noncoding RNA in cancer. *J Hematol Oncol* 2019; **12**:121.
18 Zuo X, Chen Z, Gao W, Zhang Y, Wang J, Wang J, *et al*. M6A-mediated upregulation of LINC00958 increases lipogenesis and acts as a nanotherapeutic target in hepatocellular carcinoma. *J Hematol Oncol* 2020; **13**:5.
19 Arguello AE, DeLiberto AN, Kleiner RE. RNA chemical proteomics reveals the N6-methyladenosine (m6A)-regulated protein-RNA interactome. *J Am Chem Soc* 2017; **139**:17249–17252.
20 Li Y, Xiao J, Bai J, Tian Y, Qu Y, Chen X, *et al*. Molecular characterization and clinical relevance of m6A regulators across 33 cancer types. *Mol Cancer* 2019; **18**:137.
21 Zhou Z, Lv J, Yu H, Han J, Yang X, Feng D, *et al*. Mechanism of RNA modification N6-methyladenosine in human cancer. *Mol Cancer* 2020; **19**:104.
22 Yu G, Wang LG, Han Y, He QY. clusterProfiler: an R package for comparing biological themes among gene clusters. *OMICS* 2012; **16**:284–287.
23 Walter W, Sánchez-Cabo F, Ricote M. GOplot: an R package for visually combining expression data with functional analysis. *Bioinformatics* 2015; **31**:2912–2914.
24 Geeleher P, Cox N, Huang RS. pRRophetic: an R package for prediction of clinical chemotherapeutic response from tumor gene expression levels. *PLoS One* 2014; **9**:e107468.
25 Denisenko TV, Budkevich IN, Zhivotovsky B. Cell death-based treatment of lung adenocarcinoma. *Cell Death Dis* 2018; **9**:117.
26 Tu Z, Wu L, Wang P, Hu Q, Tao C, Li K, *et al*. N6-methylandenosine-related lncRNAs are potential biomarkers for predicting the overall survival of lower-grade glioma patients. *Front Cell Dev Biol* 2020; **8**:642.
27 Fürst DO, Osborn M, Nave R, Weber K. The organization of titin filaments in the half-sarcomere revealed by monoclonal antibodies in immunoelectron microscopy: a map of ten nonrepetitive epitopes starting at the Z line extends close to the M line. *J Cell Biol* 1988; **106**:1563–1572.
28 Kim N, Hong Y, Kwon D, Yoon S. Somatic mutaome profile in human cancer tissues. *Genomics Inform* 2013; **11**:239–244.
29 Tse C, Shoemaker AR, Adickes J, Anderson MG, Chen J, Jin S, *et al*. ABT-263: a potent and orally bioavailable Bcl-2 family inhibitor. *Cancer Res* 2008; **68**:3421–3428.
30 Zimmer AS, Gillard M, Lipkowitz S, Lee JM. Update on PARP inhibitors in breast cancer. *Curr Treat Options Oncol* 2018; **19**:21.
31 Slade D. PARP and PARG inhibitors in cancer treatment. *Genes Dev* 2020; **34**:360–394.
32 Tuli R, Shiao SL, Nissen N, Tighiouart M, Kim S, Osipov A, *et al*. A phase 1 study of veliparib, a PARP-1/2 inhibitor, with gemcitabine and radiotherapy in locally advanced pancreatic cancer. *EBioMedicine* 2019; **40**:375–381.
33 de Murcia JM, Niedergang C, Trucco C, Ricoul M, Dutrillaux B, Mark M, *et al*. Requirement of poly(ADP-ribose) polymerase in recovery from DNA damage in mice and in cells. *Proc Natl Acad Sci U S A* 1997; **94**:7303–7307.
34 Thomas HD, Calabrese CR, Batey MA, Canan S, Hostomsky Z, Kyle S, *et al*. Preclinical selection of a novel poly(ADP-ribose) polymerase inhibitor for clinical trial. *Mol Cancer Ther* 2007; **6**:945–956.
35 Russell RR 3rd, Bergeron R, Shulman GI, Young LH. Translocation of myocardial GLUT-4 and increased glucose uptake through activation of AMPK by AICAR. *Am J Physiol* 1999; **277**:H643–H649.
36 Ducommun S, Ford RJ, Bultot L, Deak M, Bertrand L, Kemp BE, *et al*. Enhanced activation of cellular AMPK by dual-small molecule treatment: AICAR and A769662. *Am J Physiol Endocrinol Metab* 2014; **306**:E688–E696.
37 Santidrián AF, González-Gironès DM, Iglesias-Serret D, Coll-Mulet L, Cosialls AM, de Frias M, *et al*. AICAR induces apoptosis independently of AMPK and p53 through up-regulation of the BH3-only proteins BIM and NOXA in chronic lymphocytic leukemia cells. *Blood* 2010; **116**:3023–3032.
38 Su RY, Chao Y, Chen TY, Huang DY, Lin WW. 5-aminoimidazole-4-carboxamide riboside sensitizes TRAIL- and TNF{alpha}-induced cytotoxicity in colon cancer cells through AMP-activated protein kinase signaling. *Mol Cancer Ther* 2007; **6**:1562–1571.

39 Sauer H, Engel S, Milosevic N, Sharifpanah F, Wartenberg M. Activation of AMP-kinase by AICAR induces apoptosis of DU-145 prostate cancer cells through generation of reactive oxygen species and activation of c-Jun N-terminal kinase. *Int J Oncol* 2012; **40**:501–508.

40 Guo F, Liu SQ, Gao XH, Zhang LY. AICAR induces AMPK-independent programmed necrosis in prostate cancer cells. *Biochem Biophys Res Commun* 2016; **474**:277–283.

41 Cortes JE, Kim DW, Pinilla-Ibarz J, le Coutre P, Paquette R, Chuah C, *et al*; PACE Investigators. A phase 2 trial of ponatinib in Philadelphia chromosome-positive leukemias. *N Engl J Med* 2013; **369**:1783–1796.

42 O'Hare T, Shakespeare WC, Zhu X, Eide CA, Rivera VM, Wang F, *et al*. AP24534, a pan-BCR-ABL inhibitor for chronic myeloid leukemia, potently inhibits the T315I mutant and overcomes mutation-based resistance. *Cancer Cell* 2009; **16**:401–412.

43 Gkouveris I, Nikitakis NG. Role of JNK signaling in oral cancer: a mini review. *Tumour Biol* 2017; **39**:1010428317711659.

44 Okada M, Shibuya K, Sato A, Seino S, Watanabe E, Suzuki S, *et al*. Specific role of JNK in the maintenance of the tumor-initiating capacity of A549 human non-small cell lung cancer cells. *Oncol Rep* 2013; **30**:1957–1964.

45 Cerbone A, Toaldo C, Pizzimenti S, Pettazzoni P, Dianzani C, Minelli R, *et al*. AS601245, an anti-inflammatory JNK inhibitor, and clofibrate have a synergistic effect in inducing cell responses and in affecting the gene expression profile in CaCo-2 colon cancer cells. *PPAR Res* 2012; **2012**:269751.

46 Akita T, Horiguchi M, Ozawa C, Terada H, Yamashita C. The effect of a retinoic acid derivative on cell-growth inhibition in a pulmonary carcinoma cell line. *Biol Pharm Bull* 2016; **39**:308–312.

47 Cheng J, Qi J, Li XT, Zhou K, Xu JH, Zhou Y, *et al*. ATRA and genistein synergistically inhibit the metastatic potential of human lung adenocarcinoma cells. *Int J Clin Exp Med* 2015; **8**:4220–4227.

48 Choi YJ, Kim SY, So KS, Baek IJ, Kim WS, Choi SH, *et al*. AUY922 effectively overcomes MET- and AXL-mediated resistance to EGFR-TKI in lung cancer cells. *PLoS One* 2015; **10**:e0119832.

49 Hiscox S, Morgan L, Green TP, Barrow D, Gee J, Nicholson RI. Elevated Src activity promotes cellular invasion and motility in tamoxifen resistant breast cancer cells. *Breast Cancer Res Treat* 2006; **97**:263–274.

50 Zhao Y, Yang Y, Xu Y, Lu S, Jian H. AZD0530 sensitizes drug-resistant ALK-positive lung cancer cells by inhibiting SRC signaling. *FEBS Open Bio* 2017; **7**:472–476.